Stem Cell Research 15 (2015) 341–353

Contents lists available at ScienceDirect

Stem Cell Research

journal homepage: www.elsevier.com/locate/scr

Transplantation dose alters the dynamics of human neural stem cell engraftment, proliferation and migration after spinal cord injury

Katja M. Piltti [a,b,c,d,*], Sabrina N. Avakian [a,d,1], Gabriella M. Funes [a,d,1], Antoinette Hu [a,d], Nobuko Uchida [e], Aileen J. Anderson [a,b,c,d], Brian J. Cummings [a,b,c,d]

[a] Sue & Bill Gross Stem Cell Center, USA
[b] Physical & Medical Rehabilitation, USA
[c] Institute for Memory Impairments & Neurological Disorders, USA
[d] Anatomy & Neurobiology, University of California-Irvine, Irvine, CA 92697, USA
[e] StemCells Inc., 7707 Gateway, Newark, CA 94560, USA

ARTICLE INFO

Article history:
Received 6 January 2015
Received in revised form 13 June 2015
Accepted 13 July 2015
Available online 26 July 2015

Keywords:
hNSC
SCI
Stem cell niche dynamics
Stem cell transplantation
Cell dose
Survival
Proliferation
Migration

ABSTRACT

The effect of transplantation dose on the spatiotemporal dynamics of human neural stem cell (hNSC) engraftment has not been quantitatively evaluated in the central nervous system. We investigated changes over time in engraftment/survival, proliferation, and migration of multipotent human central nervous system-derived neural stem cells (hCNS-SCns) transplanted at doses ranging from 10,000 to 500,000 cells in spinal cord injured immunodeficient mice. Transplant dose was inversely correlated with measures of donor cell proliferation at 2 weeks post-transplant (WPT) and dose-normalized engraftment at 16 WPT. Critically, mice receiving the highest cell dose exhibited an engraftment plateau, in which the total number of engrafted human cells never exceeded the initial dose. These data suggest that donor cell expansion was inversely regulated by target niche parameters and/or transplantation density. Investigation of the response of donor cells to the host microenvironment should be a key variable in defining target cell dose in pre-clinical models of CNS disease and injury.

1. Introduction

We have previously shown that human central nervous system-derived stem cells propagated as neurospheres (hCNS-SCns) (Uchida et al., 2000) exhibit robust engraftment in the injured spinal cord niche after transplantation at acute, sub-acute or chronic stages of injury in immunodeficient rodent models (Cummings et al., 2005; Hooshmand et al., 2009; Salazar et al., 2010; Piltti et al., 2013a,b). Further, when transplanted into an immunodeficient model in which rejection of the xenograft is minimized, human cells were capable of both proliferation and extensive migration (Anderson et al., 2011), both of which are normal processes for CNS development (Lui et al., 2011; Hatten, 1999; Wilcock et al., 2007). In these paradigms, recovery of function was directly dependent on, and linearly correlated with, hCNS-SCns survival and engraftment, suggesting that integration with the host microenvironment is critical.

Stem cell responses in the host microenvironment depend on both intrinsic properties and extrinsic signals (Watt and Hogan, 2000; Jones and Wagers, 2008; Discher et al., 2009; Johnston, 2009; Voog and Jones, 2010; Wagers, 2012; Faigle and Song, 2013). Understanding the dynamics of donor cell engraftment, proliferation and migration is important for optimizing cell therapies for the injured or diseased CNS. Our recent data indicates that the spinal cord injury (SCI) microenvironment alters the dynamics of transplanted hCNS-SCns when compared to that in uninjured SCI models, suggesting that injury-induced cues and target niche availability play a role in donor cell maturation and migration (Sontag et al., 2014). Additionally, donor cells may also secrete factors that serve as extrinsic cues in a dose or density dependent manner. While it is has generally been assumed that 'more is better' in the context of pre-clinical stem cell transplantation, the capacity of the CNS niche to accommodate or provide cues for donor cell integration is unclear. Few studies have investigated the effect of unmodified human neural stem cell (hNSC) dose in CNS injury or disease models (Ostenfeld et al., 2000; Keirstead et al., 2005; Rossi et al., 2010; Darsalia et al., 2011). Further, none of these studies quantitatively investigated the effect of transplantation dose on the spatiotemporal dynamics of engraftment, or employed a model in which human cell rejection was sufficiently suppressed to permit donor cell expansion (Anderson et al., 2011). Accordingly, in this

* Corresponding author at: 2101 Gross Hall Stem Cell Center, University of California Irvine, Irvine, CA 92697, USA.
E-mail address: kpiltti@uci.edu (K.M. Piltti).
[1] Authors contributed equally.

http://dx.doi.org/10.1016/j.scr.2015.07.001

study we investigated the relationship between transplantation dose and early and long-term cell survival, proliferation, and migration as determined by unbiased stereological assessment of donor cells in the injured spinal cord of immunodeficient NOD-*scid* mice at 2 days post-transplantation (2 DPT), 2 weeks post-transplantation (WPT) and 16 WPT.

2. Materials and methods

2.1. Ethics statement

This study was carried out in accordance with Institutional Animal Care and Use Committee regulations at the University of California, Irvine.

2.2. hNSC isolation and culture

hCNS-SCns derivation, culture and characterization were as described (Uchida et al., 2000). Methods and lines used in this study are identical to those described in Cummings et al. (2005), Salazar et al. (2010), and Piltti et al. (2013a,b). Briefly, hCNS-SCns were propagated as neurospheres in X-Vivo 15 medium without phenol red (Lonza, Basel, Switzerland) supplemented with N2, bFGF, EGF, heparin, NAC, and LIF as described previously (Uchida et al., 2000; Cummings et al., 2005). Prior to transplantation, cells (passage ≤12) were dissociated into single cells and adjusted to the following densities: 10,000 (low dose), 100,000 (medium dose), 250,000 (high dose) or 500,000 (very high dose) cells per 5 μl in X-Vivo 15. The highest employed cell dose was selected based on the maximum injection volume at which neither tissue damage or behavioral deficits were observed in uninjured mice as empirically determined in pilot studies (1.25 μl/site); maximum cell packaging density was calculated based on hCNS-SCns size (100,000 cells/μl). Viability of hCNS-SCns after pre-transplantation cell prep and at the end of transplantation day (8–10 h post-cell prep) was >90% (Table S1B).

2.3. Contusion injuries and cell transplantation

Contusion SCI was followed by early chronic hCNS-SCns transplantation into the intact parenchyma, performed as described previously (Cummings et al., 2005; Salazar et al., 2010). Briefly, adult female NOD-*scid* mice (Jackson Laboratory, Sacramento, CA) were anesthetized with isoflurane (VetEquip Inc., Pleasanton, CA), received a T9 laminectomy using a surgical microscope, and a bilateral 50-kDa contusion injury using the Infinite Horizon Impactor (Precision Systems and Instrumentation, Lexington, KY). 30 d post-SCI, mice were re-anesthetized and 1.25 μl of freshly triturated hCNS-SCns suspension injected at four bilateral sites (for a total of 5 μl) 0.75 mm from midline. Two injection sites were at the posterior aspect of T8 (rostral to the site of injury), and two at the anterior aspect of T10 (caudal to the site of injury). Injections were conducted using a Nanoinjector with a micro controller (World Precision Instruments, Waltham, MA) at speed of 417 nl/min, followed by a 2 m delay before withdrawal of the needle, using pulled silicon-treated glass injection tips with a 70 μm ID and 110 μm OD (Sutter Instruments, Novato, CA). For assessing hCNS-SCns proliferation at 2 DPT or 2 WPT, the mice were injected i.p. with 50 mg/kg of BrdU (AbD Serotec, Raleigh, NC) every 12 h starting from the time of transplantation until 2 DPT or 2 WPT.

2.4. Randomization, exclusion criteria, and group numbers

Randomization for group allocation, exclusion criteria, and blinding for histological analysis were conducted as described previously (Cummings et al., 2005; Hooshmand et al., 2009; Salazar et al., 2010). Animals with unilateral bruising or abnormal force/displacement curves after contusion injury, or with a surgical note of poor initial injection due to imperfect needle penetration or back-flow during injection (by blinded surgeon) were excluded from stereological assessments (for exclusions see Fig. 1A). All dose groups in each time cohorts were conducted in parallel, that is, animals received spinal cord injuries at the same age and during the same week of surgery. All animal care, and histological processing/analysis were performed by observers blinded to experimental cohorts or groups. Final group numbers used in histological analysis are listed in Fig. 1A.

2.5. Perfusion, tissue collection, tissue sectioning and immunohistochemistry

Endpoints for assessing the dynamics of hCNS-SCns survival, proliferation and engraftment were selected based on our previous study describing the effect of SCI niche on hCNS-SCns engraftment between 1 DPT and 14 WPT (Sontag et al., 2014). Accordingly, the selected times represent the phases of early engraftment, proliferative expansion in the SCI niche, and the time at which the majority of donor cells have exited the cell cycle and differentiated. Mice were anesthetized and transcardially perfused 2 DPT, 2 WPT, and 16 WPT with 4% paraformaldehyde. The spinal cord T6–T12 segments were dissected based on dorsal spinal root counts, postfixed in 20% sucrose/4% paraformaldehyde overnight and frozen in isopentane at −65 °C. For brightfield stereology, T6–T12 segments were sectioned at 30 μm coronally using a CryoJane tape transfer system (Leica Microsystems Inc., Buffalo Grove, IL). Sections were processed for antigen retrieval using Buffer A (pH = 6) in the Retriever 2100 system (PickCell Laboratories, Amsterdam, Netherlands). For fluorescence conjugated immunohistochemistry, T6–T12 segments were sectioned at 30 μm coronally using a HM 450 microtome (ThermoScientific, Fairlawn, NJ). 2 DPT and 2 WPT cohort T6–T12 spinal segments were trimmed rostrally and caudally 4 mm from the injury epicenter before sectioning. Antibodies and dilutions used are listed in Fig. 1B.

2.6. Stereological analysis

Unbiased stereology was conducted using systematic random sampling with the optical fractionator probe, and StereoInvestigator version 9 (Micro BrightField Inc., Williston, VT). Parameters for the analysis are listed in Table S2. Fluorescence immunostained sections were analyzed from Z-stacks of 15 μm thick optical slices captured in 1 μm intervals using an ApoTome microscope (Zeiss, Maple Grove, MN) and 63× objective.

2.7. Cell migration analysis

For rostral–caudal proportional migration analysis, the number of stereologically quantified human cells located in the rostral versus caudal regions of spinal cord was compared after the sections in each spinal cord were aligned by injury epicenter, designated by the most damaged tissue section with the largest cross sectional lesion area. Maximal distance of cell migration (cell spread rostral and caudal relative to the injury epicenter) was determined by the distance between first and last spinal cord section with $SC121^+$ cells visualized using an inverted microscope (IX71, Olympus, Center Valley, PA).

2.8. Statistical analysis

All data are shown as mean ± standard error of mean (SEM). Statistical analysis was performed using Prism4 software, version 5.0 (GraphPad Software, San Diego, CA). Correlation between transplant dose and total number engrafted cells, survival/expansion, and migration/localization were assessed using Pearson correlation coefficient and linear regression analyses. Comparison of estimated total cell numbers, survival and expansion, maximal rostral–caudal migration distance, mitotic index, and proportion of apoptotic $CC3^+$, $BrdU^+$ or $Ki67^+$ human cells between the groups were analyzed either with one-way analysis of variance (1-way ANOVA) combined with Tukey's post hoc t-test, or Student's 2-tailed t-test. A p value ≤0.05 was considered to be statistically significant.

A

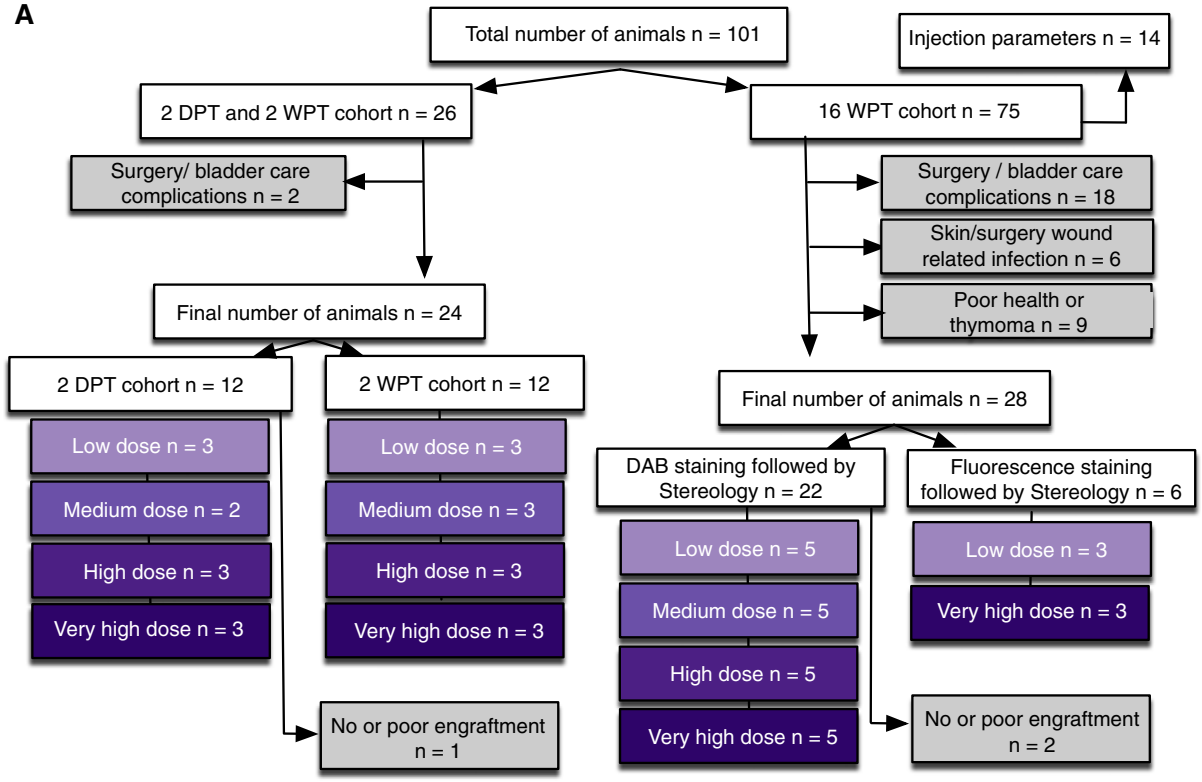

B

Antibody	Company	Dilution for DAB	Dilution for Fluorescence
Mouse anti-human-SC121 (STEM121)	StemCells	1:3000 or 1:15000	1:2000
Rat anti-BrdU	Ab Serotec	1:500	-
Rabbit anti-Ki-67	Novocastra	1:1500	1:1000
Rat anti-Histone H3 (phospho S28)	Abcam	-	1:500
Rabbit anti-cleaved caspase-3	Cell Signaling	1:5000	-
Biotin-SP-conjugated F(ab')$_2$ 2. ab	Jackson ImmunoResearch	1:500	-
Fluorescence conjugated F(ab')$_2$ 2. ab	Jackson ImmunoResearch	-	1:500

Fig. 1. Exclusions, final group numbers, and antibodies used in the study. (A) Group Ns (purple boxes) and exclusions (gray boxes) of the animals entering the study. Of note thymomas and other health complications increase dramatically with age in NOD-scid animals (Prochazka et al., 1992), resulting in an average lifespan of ~7 months of age, and a relatively high exclusion rate in the delayed transplantation paradigm employed here. Additionally, all animals were carefully screened before the study. Exclusions based on physiological phenotypes and not surgical, health, or other complications are described below for completeness (not included in A). Two physiological phenotypes resulted in a large number of exclusions. First, animals with a physical defect, such as tail malformation or missing toe (n = 2). Second, a proportion of mice (n = 19) exhibited stereotyped behavioral events consistent with a seizure disorder during handling. Events resulting in exclusion included freezing and facial movements characteristic of Racine Stage 1. The phenotype was not specific to either surgery or transplantation; however, because the potential effect of these events on transplanted cells is unknown, all mice received additional monitoring, and any animals in which repeated events (> 4) were observed were excluded from the study (n = 10). (B) Antibodies and dilutions used for DAB or fluorescence immunohistochemistry. Mayer's hematoxylin solution (Sigma-Aldrich) or Hoechst 33342 (Invitrogen) was used for nuclear labeling.

3. Results

3.1. hCNS-SCns engraftment and apoptosis 2 days post-transplant (DPT), 2 weeks post-transplant (WPT) and 16 WPT

hCNS-SCns transplanted in the early chronic stage 30 days post-SCI at doses of 10,000 (low), 100,000 (medium), 250,000 (high) or 500,000 cells (very high) exhibited robust engraftment in NOD-*scid* mice (Fig. 2A). 94.2% of all transplanted mice (n = 49/52 animals) showed engraftment of human cells, based on immunohistochemistry for the human-specific cytoplasmic marker SC121 (Fig. 2A). One animal in the low dose group and another in the medium dose group in the 16 WPT cohort showed no engraftment, which may have been due to failure during the transplant injection; these animals were excluded from further analysis. Cohort and group numbers for stereological analysis were as described in Materials and methods and in Fig. 1A. Detailed histological analysis of spinal cord tissue showed no evidence of tumor formation in any dose groups at any time points.

Based on our earlier data, hCNS-SC engraftment is not remarkably changed by proliferation or cell death within the first week post-transplantation (Sontag et al., 2014). To assess relationships between hCNS-SCns dose and human cell integration in the injured spinal cord, we carried out unbiased stereological analysis of the total numbers of SC121$^+$ human cells at 2 WPT and 16 WPT. At 2 WPT, the estimated numbers of hCNS-SCns ranged from 2877 cells in the low dose group to 44,215 cells in the very high dose group (Fig. 2B, colored bars). hCNS-SCns number increased significantly, and was positively correlated with transplant dose (Fig. S1A, Pearson r = 0.74, $^{***}p \leq 0.0003$). In

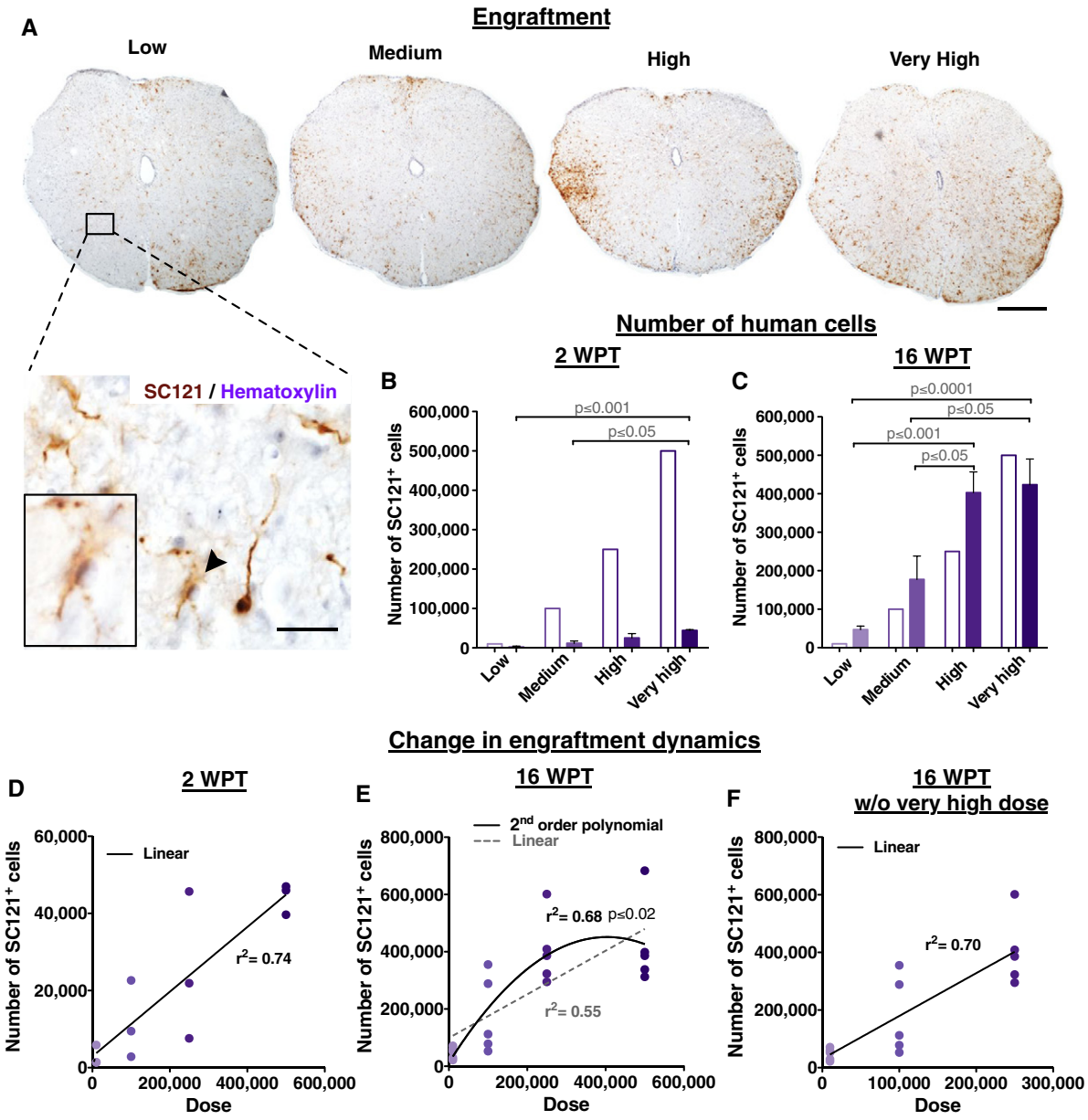

Fig. 2. Transplantation of hCNS-SCns at early chronic stage of SCI results in linear engraftment in relation to the initial transplantation dose. (A) An example of a coronal spinal cord section in each dose group after immunostaining for the human specific cytoplasmic marker SC121 (brown DAB) and hematoxylin. Scale bars 300 μm (low mag) and 50 μm (high mag). Estimated total number of hCNS-SCns positive for SC121 (bars shaded to indicate dose) were significantly greater in the very high dose group when compared to the low or medium dose groups (B) at 2 WPT or (C) 16 WPT; mean ± SEM, 1-way ANOVA $p = 0.009$ (previously published in Piltti et al., submitted for publication) and 1-way ANOVA $p = 0.0002$, respectively. Tukey's t-test p values are shown in the graphs. (D) Comparative analysis revealed no significant improvement in goodness of fit when a second order polynomial versus a first order linear fit was applied to the data set at 2 WPT; Extra Sum of Squares F test $p \leq 0.79$, $n = 3$/group. However, (E) a significant improvement in goodness of fit when a second order polynomial versus a first order linear fit was applied to the data set containing all dose groups, suggesting an engraftment plateau at 16 WPT; Extra Sum of Squares F test $p \leq 0.02$, $n = 5$/group. (F) This was not apparent when the very high dose group was eliminated from the 16 WPT dataset; $p \leq 0.96$, $n = 5$/group (previously published in Piltti et al., submitted for publication). 2 WPT cohort $n = 3$ animals/group, 16 WPT cohort $n = 5$ animals/group.

parallel, at 16 WPT, the estimated number of hCNS-SCns ranged from 46,932 cells in the low dose group to 423,554 cells in the very high dose group (Fig. 2C). Again, hCNS-SCns number increased significantly, and was positively correlated with transplant dose (Fig. S1B, Pearson $r = 0.74$, $^{***}p \leq 0.0002$). These data suggest that the total number of human cells in the injured spinal cord is linearly related to the initial transplantation dose. However, the number of human cells present at 16 WPT appeared to plateau at higher doses (Fig. 2C). Comparative analysis revealed a significant improvement in goodness of fit when a second order polynomial versus a first order linear fit was applied to the data set containing all dose groups (Fig. 2E; Extra Sum of Squares F test $p \leq 0.02$), which was not apparent at 2 WPT (Fig. 2D; Extra Sum of Squares F test $p \leq 0.79$) or when the very high dose group was eliminated from the 16 WPT dataset (Fig. 2F; Extra Sum of Squares F test $p \leq 0.96$). These data support a change in engraftment dynamics between the 'high' and 'very' high dose groups, resulting in an engraftment plateau between 2 WPT and 16 WPT. Finally, the low number of surviving donor cells at 2 WPT indicates that a large fraction of the initial transplant was lost, as previously reported.

3.2. hCNS-SCns survival and expansion between 2 and 16 WPT

To assess early hCNS-SCns survival, we conducted double-labeling immunohistochemistry for SC121 and the apoptotic marker cleaved caspase 3 (CC3) at 2 days post-transplantation (DPT), 2 weeks post-transplantation (WPT) and 16 WPT, as illustrated in Fig. 3A. Apoptosis

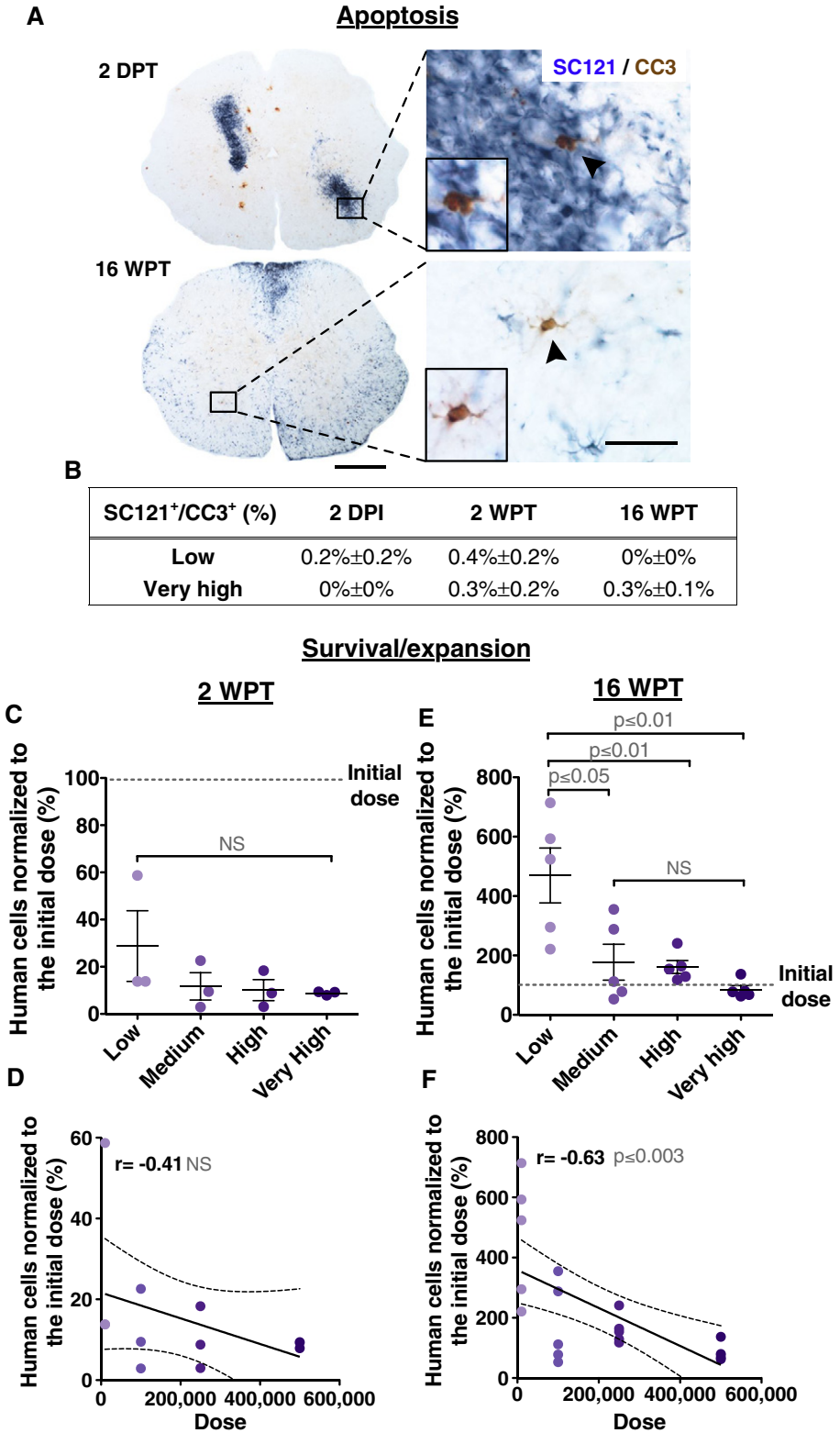

SC121⁺/CC3⁺ (%)	2 DPI	2 WPT	16 WPT
Low	0.2%±0.2%	0.4%±0.2%	0%±0%
Very high	0%±0%	0.3%±0.2%	0.3%±0.1%

Fig. 3. Transplant dose does not alter early cell survival but has an inverse effect long term on donor cell survival/expansion (16 WPT). (A) An example of spinal cord sections immunostained for SC121 and cleaved caspase-3 (CC3) showing that few human cells were undergoing apoptosis (arrows) at 2 DPT or 16 WPT. Scale bars 300 μm (low mag) and 20 μm (high mag). (B) No significant differences were found in the proportion of $SC121^+/CC3^+$ cells between low and very high dose groups at 2DPT, 2 WPT or 16 WPT; Student's 2-tailed t-test $p \leq 0.4$, $p \leq 0.5$ or $p \leq 0.2$ respectively, n = 3 animals/group. hCNS-SCns cell survival and expansion rate per dose group in the injured spinal cords after the total numbers of $SC121^+$ human cells were normalized with the initial transplantation doses at (C) 2 WPT or (E) 16 WPT; mean ± SEM, 1-way ANOVA $p = 0.35$; 1-way ANOVA $p = 0.001$, respectively. Tukey's t-test p values are shown in the graph, as are individual data points in each dose group (dots shaded to indicate dose) and the initial transplantation dose (dashed line). Correlation coefficients revealed no relationship between cell dose and survival at 2 WPT (D) but there was an inverse correlation between dose and donor cell expansion magnitude at 16 WPT (F); Pearson $r = -0.41$, $p \leq 0.18$; Pearson $r = -0.63$, $p \leq 0.003$, respectively. XY scatterplots data points/group (dots) and regression line ± SEM. 2 WPT cohort $n = 3$ animals/group, 16 WPT cohort $n = 5$ animals/group.

has been suggested to be a predominant mechanism of cell death following neural stem cell xenotransplantation in immunosuppressed injury models (Bakshi et al., 2005). However, in our study, very few SC121$^+$ human cells in any dose group or time point assessed expressed CC3, and no significant differences were found between low and very high dose groups at any time points (Fig. 3B). Critically, hCNS-SCns survival was not significantly decreased as a part of the process of cell preparation for transplantation, as >90% viability is observed before and 8–10 h post-cell preparation (Table S1B). These data therefore suggest that hCNS-SCns loss was likely to occur shortly after or during the transplantation process, likely as a result of mechanical shear forces during injection (Aguado et al., 2012).

In our previous studies, hCNS-SCns transplanted at a dose of 75,000 cells exhibited an average of 250% expansion over the initial transplantation dose in this immunodeficient mouse SCI model by 12–16 WPT (Cummings et al., 2005; Hooshmand et al., 2009; Salazar et al., 2010; Sontag et al., 2013, 2014). To test the effect of dose on donor cell survival/expansion, we normalized the stereologically quantified number of human cells present to the initial transplantation dose to obtain the proportion of surviving cells at 2 and 16 WPT. At 2 WPT this value ranged from 28.8% in the low dose group to 8.8% in the very high dose group. No significant difference was found between dose groups (Fig. 3C), and no correlative relationship was detected between dose and survival (Fig. 3D). In contrast, at 16 WPT significant differences between dose and expansion were observed. The expansion value ranged from 469% in the low dose group to 85% in the very high dose group (Fig. 3E). Although the very high dose group showed the greatest numbers of SC121$^+$ human cells, the expansion magnitude was significantly greater in the low dose group (Fig. 3E), and there was an inverse correlation between increasing dose and expansion magnitude (Fig. 3F). This observation was also true if expansion magnitude was determined by normalizing the stereologically quantified number of donor cells present 16 WPT to the number of surviving donor cells present at 2 WPT. Surprisingly, these data suggest a 15–16 fold expansion of cell number in the low, medium and high dose groups (Fig. 4A). Importantly, however, while this is a striking degree of donor cell expansion in the host microenvironment, a geometric model predicts that only four divisions of each surviving human cell at 2 WPT would be sufficient to result in the numbers detected at 16 WPT (Fig. 4B).

3.3. hCNS-SCns migration kinetics/dynamics

We have previously reported that hCNS-SCns transplantation in NOD-scid SCI model 9 days post-injury (dpi) resulted in an equivalent distribution of donor cells rostral and caudal to the epicenter that was irrespective to the time of post-transplantation assessment; 1, 7, 14, 28 or 96 DPT. However, hCNS-SCns transplantation in the same SCI model 30 dpi resulted in increased cell localization in the region rostral to the epicenter as previously detected (Salazar et al., 2010), suggesting that cell migration/proliferation cues within the injured tissue may change in a time dependent manner. 3D reconstruction of the localization of donor cells based on stereological quantification of the number of SC121$^+$ human cells at 2 WPT (14 DPT) and 16 WPT (96 DPT) revealed a strong localization to the region rostral to the epicenter (Fig. 5A–B, Movies S1–4). To measure the effect of transplant dose on rostral or caudal proportional migration of donor cells, we compared the number of stereologically quantified human cells located in the rostral versus caudal regions of spinal cord sections aligned by the injury epicenter

A

Dose group	2 WPT SC121$^+$ cells ± SEM	16 WPT SC121$^+$ cells ± SEM	Increase (%)	Fold increase
Low (10K)	2,877 ± 1,496	46,932 ± 9,226	1.631	16.3
Medium (100K)	11,649 ± 5,808	177,324 ± 60,688	1.522	15.2
High (250K)	25,067 ± 11,108	402,919 ± 53,734	1.607	16.1
Very high (500K)	44,215 ± 2,289	423,554 ± 66,704	958	9.6

B

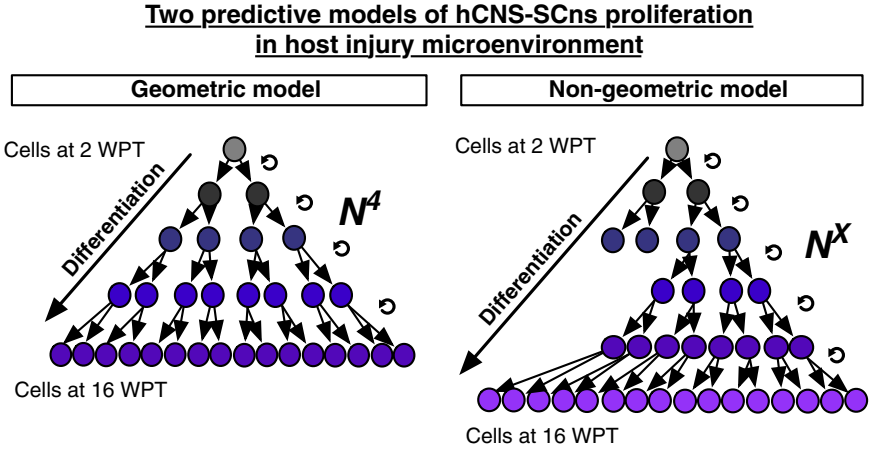

Fig. 4. hCNS-SCns expansion in the host injured spinal cord. (A) Increase in numbers of hCNS-SCns in host injury microenvironment at 2 WPT and 16 WPT. Mean ± SEM, 2 WPT cohort $n = 3$ animals/group, 16 WPT cohort $n = 5$ animals/group. (B) A geometric proliferation model predicts that only four divisions (N^4) of each surviving human cell at 2 WPT would be sufficient to result in the numbers detected at 16 WPT. Alternatively, a non-geometric proliferation model predicts that more than four cell divisions (N^X) would be needed to produce the numbers detected at 16 WPT.

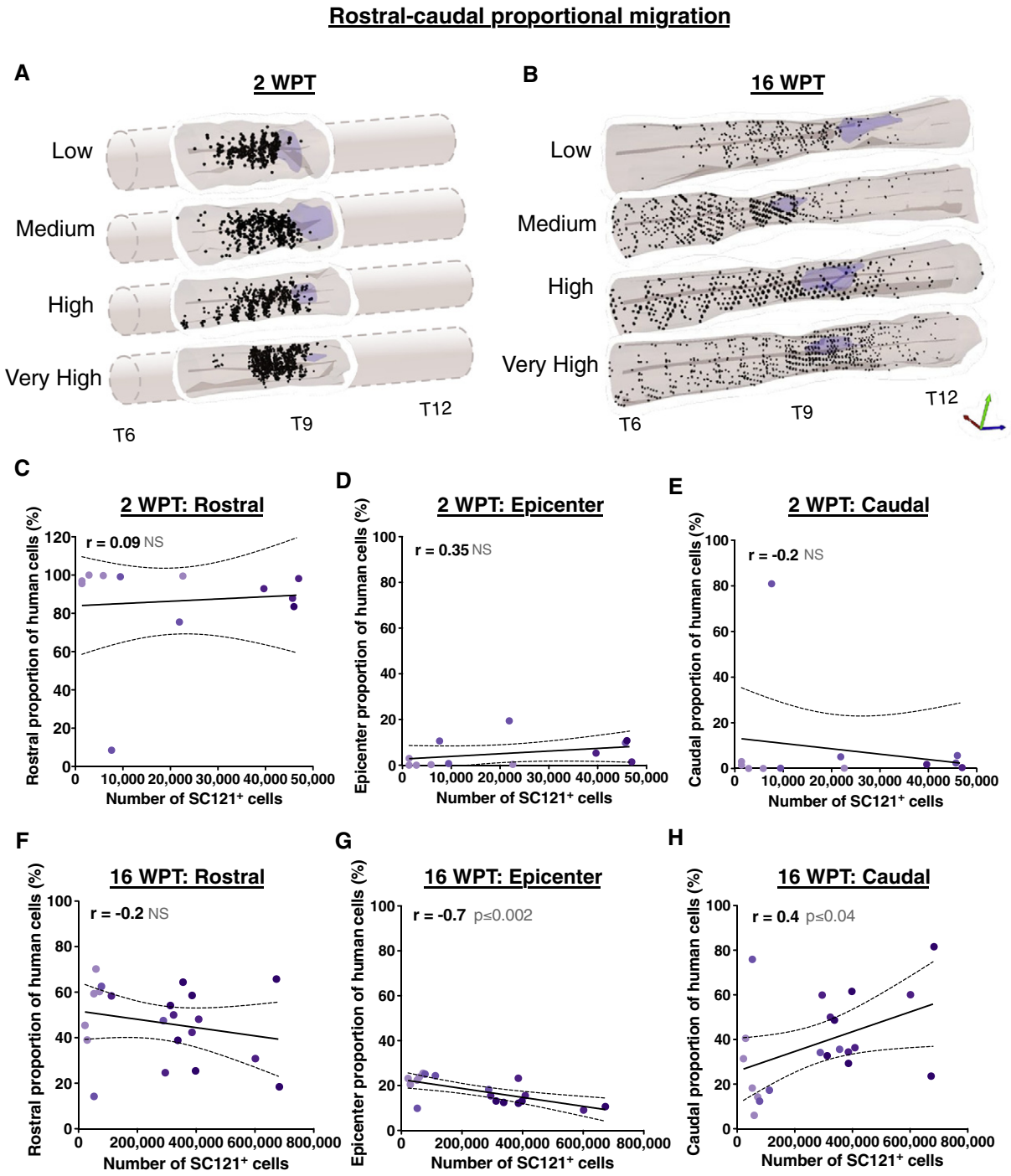

Fig. 5. Effect of transplant on rostral–caudal proportional migration in the injured spinal cord niche. 3D reconstructions of transplanted spinal cords illustrating the location of analyzed $SC121^+$ human cells (dots shaded to indicate dose) relative to the lesion area (purple shaded area) at 2 WPT (A) or 16 WPT (B) show a strong preference of hCNS-SCns for rostral regions after early-chronic transplantation. At 2 WPT, correlation analyses revealed no dose-dependent relationship in rostral (C), epicenter (D), or caudal (E) localization of donor cells; Pearson $r = -0.09$, $p \le 0.8$; $r = 0.35$, $p \le 0.3$; $r = -0.19$, $p \le 0.5$, respectively. However, at 16 WPT, although there was no dose-dependent relationship in rostral (F) localization of donor cells, increasing cell dose exhibited a negative correlation with epicenter (G) localization, and a positive correlation with caudal (H) localization, suggesting that increasing transplantation dose increased caudal donor cell migration; Pearson $r = -0.2$, $p \le 0.3$; $r = -0.69$, $p \le 0.002$; $r = 0.45$, $p \le 0.04$, respectively. XY scatterplots of data points/group (colored dots) and regression line ± SEM. 2 WPT cohort n = 3 animals/group, 16 WPT cohort n = 5 animals/group.

as designated by the most damaged tissue section with largest cross sectional lesion area. Correlation analyses revealed no total human cell number-dependent relationship in the rostral, epicenter, or caudal localization of donor cells 2 WPT (Fig. 5C–E), or in rostral localization 16 WPT (Fig. 5F). In contrast, engrafted human cell number exhibited a inverse correlation with epicenter localization (Fig. 5G), and a positive correlation with caudal localization (Fig. 5H) 16 WPT. These data suggest that delayed transplantation was associated with early preferential localization of donor cells to regions rostral to the injury, and that increasing dose in this paradigm expanded the migration of cells to caudal areas by 16 WPT.

To investigate the kinetics of human cell migration in the injured spinal cord, we next asked whether donor cell dose affected maximal rostral–caudal migration; that is, the distance between the farthest

observed rostral and caudal donor cells. We expanded our analysis of early engraftment time points to include 2 DPT, and determined the distance between the first and last spinal cord section in which SC121$^+$ human cells were found at 2 DPT, 2 WPT and 16 WPT. At 2 DPT, the majority of hCNS-SCns were located near the four injection sites, and there was a significant increase in the maximal rostral–caudal migration of donor human SC121$^+$ cells in the very high versus low dose groups (Fig. 6A). This observation was paralleled at 2 WPT, with a significant increase observed between both the high and very high versus low dose groups (Fig. 6B). In accordance, a significant positive correlation was found between dose and maximal rostral–caudal migration at 2 DPT and 2 WPT (Fig. 6D–E). However, neither the quantitative nor the correlative differences between dose and maximal rostral–caudal migration were sustained at 16 WPT (Fig. 6C and F).

Based on the observed preferential rostral localization of donor cells in the early post-transplantation period, we further assessed migration in the parenchyma by specifically testing rostral *versus* caudal migration relative to the injury epicenter. There was a significant relationship between dose and maximal caudal migration at 2 DPT (Fig. 6G), and maximal rostral migration at 2 WPT (Fig. 6H). However, no correlative relationships were observed at 16 WPT (Fig. 6I). Taken together, these data demonstrate a dose dependent increase in the number of cells localized in the caudal niche at 16 WPT, despite the fact that cells in the low dose group were capable of comparable maximal migration in the injured spinal cord.

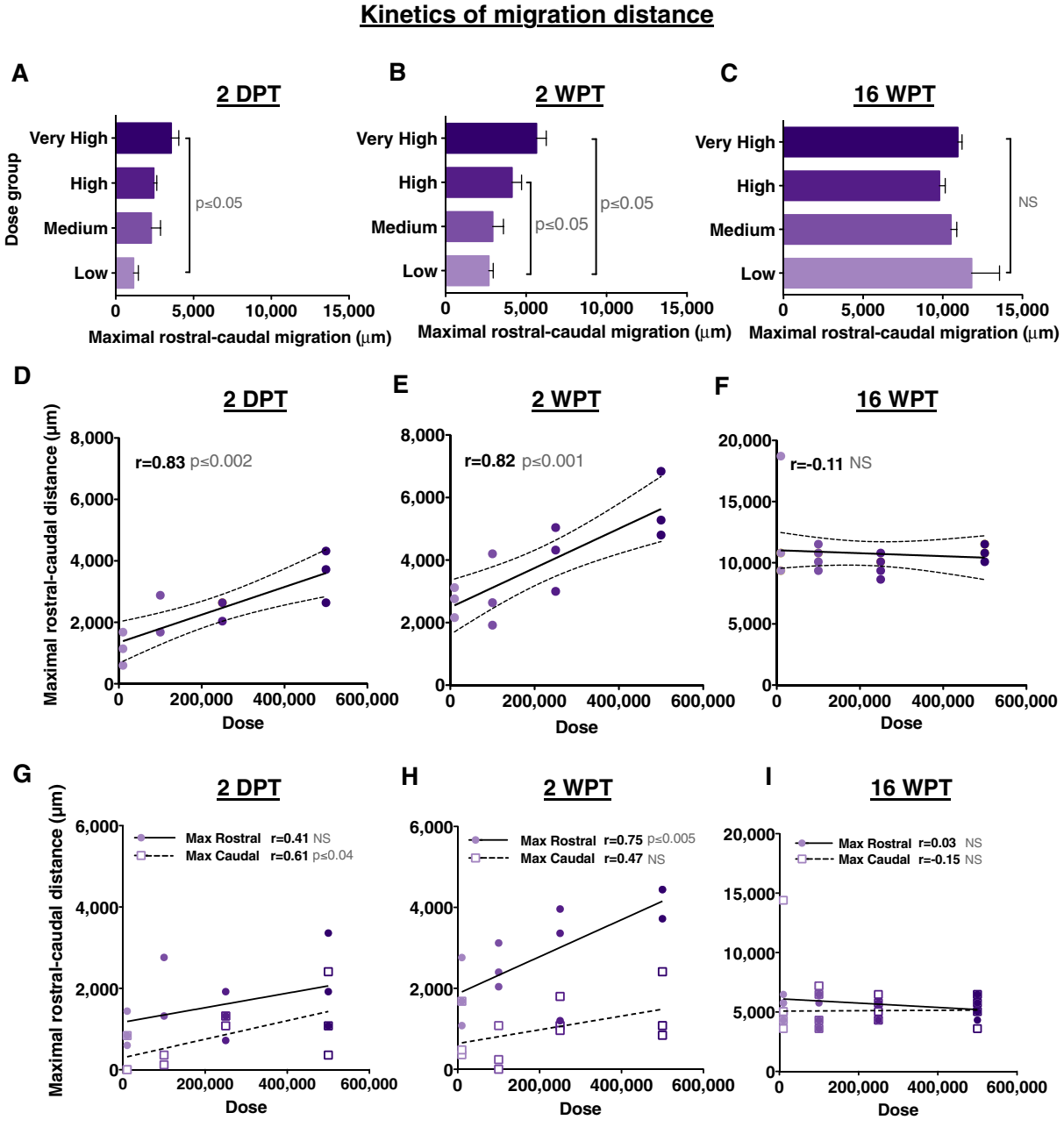

Fig. 6. Transplant dose has a transient effect on maximal rostral–caudal migration of donor cells in the injured spinal cord niche. Maximal rostral–caudal migration of human SC121$^+$ cells at (A) 2 DPT, (B) 2 WPT or (C) 16 WPT; mean ± SEM, 1-way ANOVA $p = 0.02$; $p = 0.02$, $p = 0.49$, respectively. Tukey's t-test p values are shown in the graph. Correlation analysis revealed that increasing cell dose exhibited a linear correlation with maximal cell spread at (D) 2 DPT and (E) 2 WPT but not at (F) 16 WPT; Pearson $r = 0.83$, $p \le 0.002$; $r = 0.82$, $p \le 0.001$; Pearson $r = -0.11$, $p \le 0.63$, respectively. Correlation analysis between transplant dose and maximal migration distance in the rostral or caudal regions at (G) 2 DPT; Pearson $r = 0.61$, $p \le 0.04$, $r = 0.41$, $p \le 0.2$; (H) 2 WPT; Pearson $r = 0.75$, $p \le 0.005$, $r = 0.47$, $p \le 0.12$; or (I) 16 WPT; Pearson $r = 0.03$, $p \le 0.88$, $r = -0.15$, $p \le 0.54$. XY scatterplots of data points/group (dots shaded to indicate dose) and regression line ± SEM. 2DPT and 2 WPT cohorts $n = 3$ animals/group, 16 WPT cohort $n = 5$ animals/group.

3.4. hCNS-SCns proliferation at 2 DPT and 2 WPT

We have previously demonstrated that hCNS-SCns proliferation underlies donor cell expansion, that proliferation occurs in the early post-transplantation period and is altered by the injured niche, and that the proportion of human cells actively proliferating by 12 WPT has declined to 1–2% (Sontag et al., 2014). Because low cell dose groups exhibited greater expansion in the SCI niche, we tested the effect of cell dose on hCNS-SCns proliferation using a cumulative BrdU labeling paradigm. For this study, mice received i.p. injections of BrdU twice a day beginning at the time of transplantation. BrdU incorporation was found in both donor and endogenous cells as expected based on previous characterizations (McTigue et al., 2001); donor cells were therefore identified by double labeling for SC121 and BrdU. At 2 DPT (Fig. S2A) or 2 WPT (Fig. 7A), the majority of the $SC121^+/BrdU^+$ cells were located near the injection sites in all dose groups. At 2 WPT the total number of $SC121^+/BrdU^+$ cells ranged from 2493 in the low dose group to 17,946 in the very high dose group, with a significant increase detected between these groups (Fig. 7B). These data suggest that the total number of $BrdU^+$ human cells increased with increasing cell dose.

However, evaluation of the effect of cell dose on the proportion of human cells that exhibited BrdU incorporation revealed a more complex relationship. At 2 DPT the proportion of donor cells incorporating BrdU in the injured niche was low (8%–2.9%) with no significant difference between the low and very high dose groups (Fig. S2B). In contrast, at 2 WPT, 84.2% of cells in the low dose group exhibited BrdU incorporation, while only 41.7% of cells in the very high dose group did so (Fig. 7C), and an inverse correlation was observed between the total number of engrafted human cells and the proportion of $SC121^+/BrdU^+$ cells (Fig. 7D). Alignment of spinal cord sections relative to the injury epicenter revealed a preferential rostral localization of $SC121^+/BrdU^+$ cells at 2 WPT that was not affected by the total number of engrafted human cells (Fig. 7E, Fig. S2C and Movies S5–6; Fig. 7F–H). These data suggest the surprising finding that increasing dose exerted an inverse effect on donor cell proliferation in the SCI microenvironment between 2 DPT and 2 WPT, but do not support a regional specificity in proliferation with respect to dose.

3.5. hCNS-SCns proliferation 16 WPT

We investigated the relationship between transplantation dose and markers associated with long-term donor cell proliferation at 16 WPT using double labeling immunohistochemistry for SC121 and Ki67. As shown in Fig. 8A, $Ki76^+$ nuclei exhibited either solid nucleoplasmic or dotted mid-G1 phase-like staining (Kill, 1996), both of which were included in unbiased stereological quantification. Labeling of endogenous mouse cell nuclei was also observed. The estimated total number of $SC121^+/Ki67^+$ cells ranged from 10,470 in the low dose group to 70,117 in the very high dose group, with a significant increase in the high and very high dose groups (Fig. 8B) compared to the low dose group.

The proportion of $SC121^+/Ki67^+$ cells ranged from 23.3% in the low dose group to 16.5% in the very high dose group, with no significant difference between the groups (Fig. 8C). However, as in the case of BrdU analysis at early post-transplantation time points, there was an inverse correlation between the total number of engrafted human cells and the proportion of $SC121^+/Ki67^+$ cells (Fig. 8D), consistent with the increased cell expansion observed in the low dose group. Further, alignment of spinal cord sections relative to the injury epicenter again revealed a preferential rostral localization of $SC121^+/Ki67^+$ donor cells rostral to the injury epicenter (Fig. 8E, Movies S7–8); however, although there were no significant overall differences between dose groups (Fig. S2D), there was a specific and significant inverse correlation between the total number of engrafted human cells and rostral localization of $SC121^+/Ki67^+$ cells (Fig. 8F–H). These data support a sustained inverse effect of dose on donor cell proliferation in the SCI microenvironment extending through 16 WPT, and suggest that regional differences in proliferation dynamics emerge over time.

Ki67 labeling detects cells in G1, S, G2 and M phase, and therefore can significantly overestimate the number of cells in active mitosis (Kill, 1996; Tanaka et al., 2011). We therefore sought to determine what proportion of $Ki67^+$ cells were in active cell division using Phospho-Histone-3 (pH3), a specific M phase marker (Gurley et al., 1978; Shibata and Ajiro, 1993; Hendzel et al., 1997). Triple labeling immunohistochemistry for $SC121^+/Ki67^+/pH3^+$ cells (Fig. S3) demonstrated that the fraction of mitotic $pH3^+$ cells within the $SC121^+/Ki67^+$ population ranged from 10.3% in the low dose group to 4.8% in the very high dose group with no significant difference between the groups (1-way ANOVA $p = 0.08$). Proportional analysis relative to the total number of $SC121^+$ human cells revealed that transplanted hCNS-SCns exhibited a mitotic index of 1–3% at 16 WPT (depending on dose), consistent with previous observations from our laboratory at a dose of 75,000 cells (Salazar et al., 2010; Sontag et al., 2014).

4. Discussion

Cellular therapeutics may function via either replacement of a lost cell population (e.g. generation of new dopamine neurons or myelinating oligodendrocytes), restoration of a cellular function (e.g. synthesis/secretion of an enzyme in the case of a genetic deficiency), or modulation of the host microenvironment (e.g. attenuation of an autoimmune response). Cell replacement/restoration requires long term functional integration of the donor cell population. However, the effect of transplant dose on donor cell integration has been characterized only in hematopoietic stem cells (HSC), where the magnitude of human HSC engraftment and rate of donor cell mobilization is proportional to transplant dose (Chen et al., 2004; Liu et al., 2010). However, donor-derived progeny in peripheral blood increases over time irrespective of transplant dose (Chen et al., 2004; Liu et al., 2010), indicating that the dynamics of engraftment in the stem cell niche may be a key factor in successful cell replacement. Additionally, HSC have been reported to fail multi-lineage development when transplanted at ultra low density (Liu et al., 2010), making assessment of dose-related integration into the niche an important variable. In this regard, while it has generally been assumed that "more is better", the capacity of the injured CNS to provide integration sites after therapeutic transplantation is unknown. Accordingly, we investigated relationship between the number of transplanted hCNS-SCns (dose) and the spatiotemporal dynamics of early and long-term cell survival, proliferation, and migration in the SCI microenvironment.

Few previous studies have investigated the effect of unmodified human neural stem cell/precursor dose in CNS injury or disease models. A linear relationship between the number of transplanted human neural precursors (200,000–2,000,000 cells) and graft volume was reported in a rat Parkinson's disease (PD) model (Ostenfeld et al., 2000), but not in a rat stroke model, in which increasing hNSC dose (300,000–1,500,000 cells) did not significantly increase engraftment (Darsalia et al., 2011). The variation in outcome between these studies may be due to differences in the diseased versus injured niche, use of different transplantation paradigms, and critically, differences in whether adequate pharmacological immunosuppression was achieved in these respective xenotransplantation models. In this regard, lack of adequate immunosuppression could lead to a dose-dependent increase in immune rejection. In our study, similar to HSC and the PD model above, increasing hCNS-SCns dose (10,000–250,000 cells) exhibited a linear relationship with the total number of engrafted donor cells, suggesting that human cell engraftment was scalable within the SCI niche. However, the highest hCNS-SCns dose (500,000 cells) exhibited a plateau in donor cell engraftment, suggesting that the SCI niche does have a limit to its capacity to accommodate/integrate donor cells. Because previous studies (Ostenfeld et al., 2000; Keirstead et al., 2005; Rossi et al., 2010; Darsalia et al., 2011) have not conducted complete analyses of cell engraftment, it is unclear whether a similarly complex relationship encompassing both a linear increase in

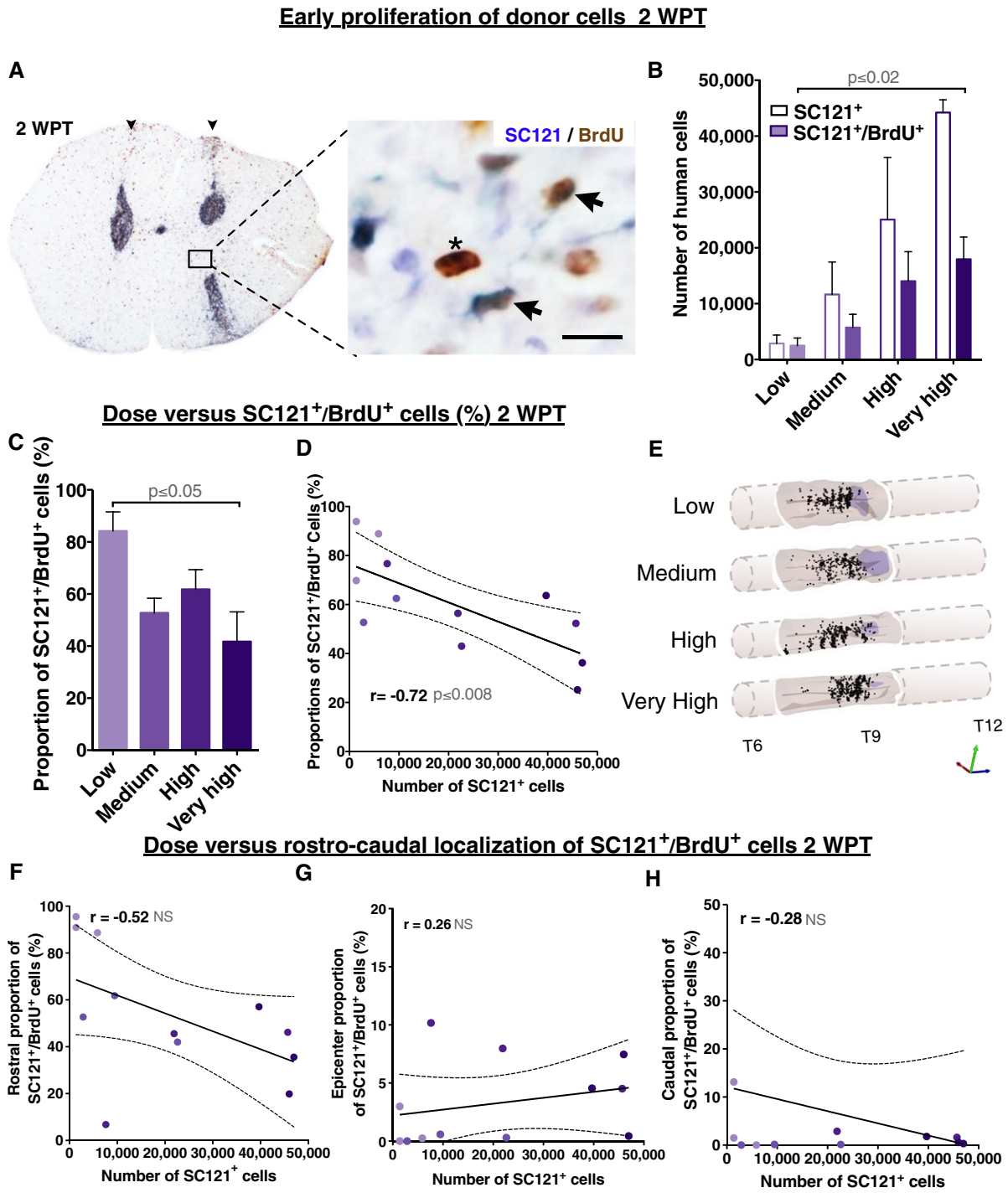

Fig. 7. Transplantation dose has an inverse effect on hCNS-SCns proliferation at 2 WPT. (A) An example of coronal spinal cord section immunostained for a human marker SC121 (blue DAB) and BrdU (brown DAB) at 2 WPT. Photomicrograph of bilateral injection tracts (arrowheads), $SC121^+/BrdU^+$ cells (arrows), and an endogenous $BrdU^+$ cell (asterisk). Inset scale bar 10 μm. (B) The very high dose group showed significantly greater estimated total number of $SC121^+/BrdU^+$ cells (colored bars shaded to indicate dose) when compared to low dose group at 2 WPT; mean ± SEM, 1-way ANOVA $p \leq 0.05$. Student's 2-tailed t-test p value is shown in the graph. Colored outlines of the initial number of $SC121^+$ cells/group. However, (C) normalization with the total number of human cells revealed that the low dose group exhibited a significantly greater proportion of $SC121^+/BrdU^+$ cells when compared to the very high dose group; mean ± SEM, 1-way ANOVA $p \leq 0.03$. Tukey's t-test p value is shown in the graph. In accordance, correlation coefficients revealed a significant negative correlation between higher total number of $SC121^+$ donor cells and greater proportion of $SC121^+/BrdU^+$ cells; Pearson $r = -0.72$, $p \leq 0.008$. (E) 3D reconstruction of transplanted spinal cords showing location of analyzed $SC121^+/BrdU^+$ cells (dots) in each dose group at 2 WPT. The purple shaded area represents the lesion. Correlation analysis between transplant dose and proportion of $SC121^+/BrdU^+$ cells localized in (F) the rostral region; Pearson $r = -0.52$, $p \leq 0.08$; the epicenter (G); $r = 0.26$, $p \leq 0.4$, or (H) the caudal region; $r = -0.28$, $p \leq 0.38$. XY scatterplots data points/group (dots shaded to indicate dose) and regression line ± SEM. 2 WPT cohort $n = 3$ animals/group.

engraftment with increasing cell dose and a plateau in this relationship also exists in the injured/diseased brain as a transplantation niche.

Although only a small proportion of cells (9–29%) survived the transplantation process, which is in accordance with our previous data (Sontag et al., 2014), there was no significant relationship between the proportion of dying cells and transplantation dose. The lack of dose-related cell death may suggest that donor cell proliferation is regulated by cell density or density-dependent access to local nutrients and

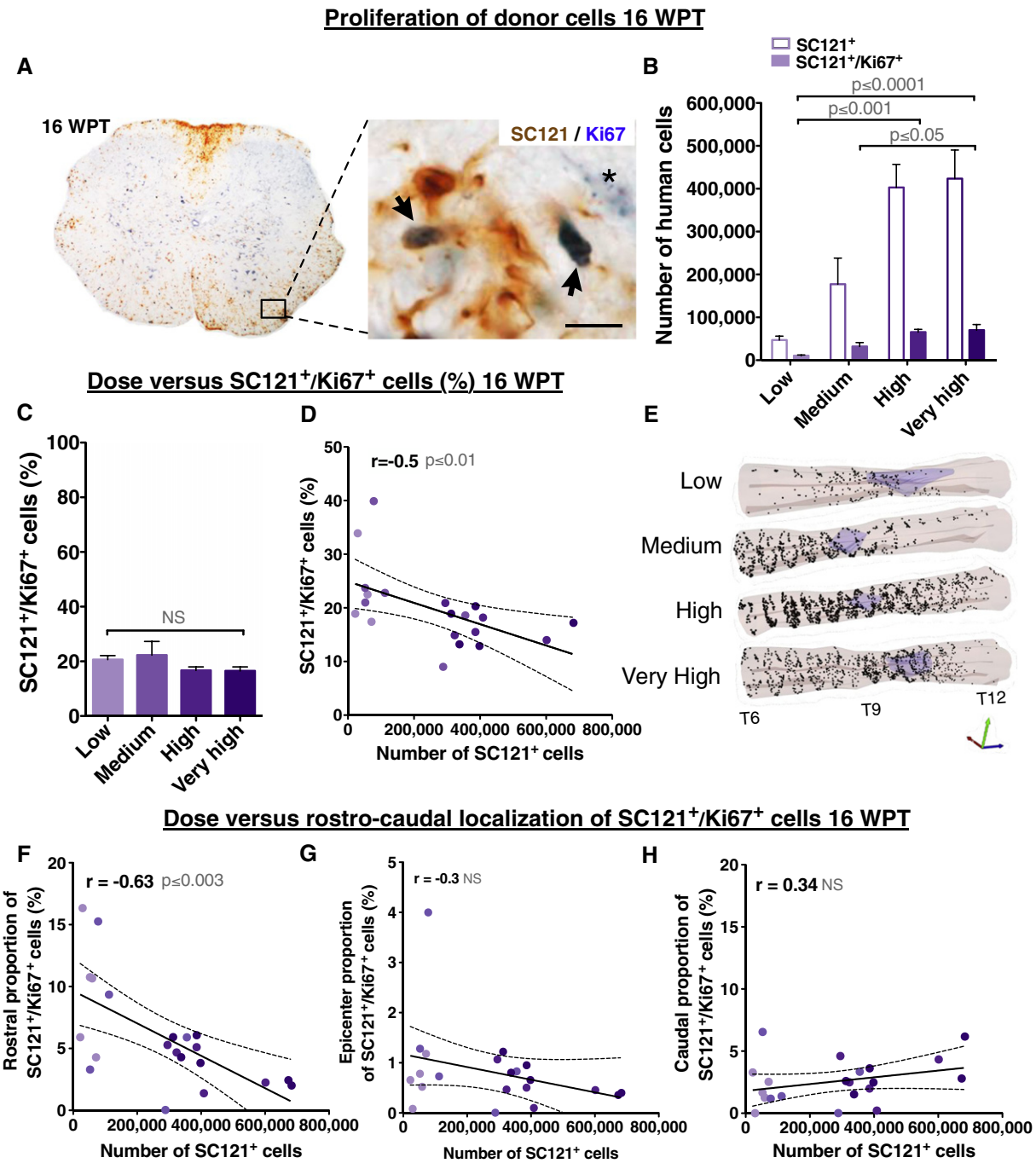

Fig. 8. Donor cells proliferation is dramatically decreased in the injured spinal cords between 2 WPT and 16 WPT. (A) An example of a coronal spinal cord section immunostained for human marker SC121 (brown DAB) and Ki67 (blue DAB) at 16 WPT depicting human SC121$^+$/Ki67$^+$ cells (arrows) and an endogenous cell with a dotted G1 interphase stage-like Ki67$^+$ staining (asterisk). Inset scale bar 10 μm. (B) Very high and high dose groups exhibited significantly greater estimated total number of SC121$^+$/Ki67$^+$ human cells (colored bars shaded to indicate dose) compared to the low dose groups; mean ± SEM, 1-way ANOVA $p = 0.0004$. Tukey's t-test p values are shown in the graph. Colored outlines of the initial dose of SC121$^+$ cells. (C) No difference was found between the proportion of SC121$^+$/Ki67$^+$ cells in each dose group after normalization to the total number of SC121$^+$ cells (previously published in Piltti et al., submitted for publication); mean ± SEM, 1-way ANOVA $p = 0.28$. However, (D) correlation analysis revealed a significant negative relationship between increasing cell dose and the proportion of SC121$^+$/Ki67$^+$ donor cells; Pearson $r = -0.55$, $p \leq 0.01$. (E) 3D reconstruction of transplanted spinal cords showing location of analyzed SC121$^+$/Ki67$^+$ cells (dots) at 16 WPT. urple shaded area represents the lesion. (F) Correlation analysis between transplant dose and proportion of SC121$^+$/Ki67$^+$ cells localized in (F) the rostral region; Pearson $r = -0.63$, $p \leq 0.003$; (G) the epicenter; $r = -0.3$, $p \leq 0.2$, or (H) the caudal region; $r = 0.34$, $p \leq 0.1$. XY scatterblots data points/group (dots shaded to indicate dose) and regression line ± SEM. 16 WPT cohort $n = 5$ animals/group.

growth factors/signals (Discher et al., 2009; Gomer et al., 2011; Brizzi et al., 2012). In this context, inclusion of a transplantation matrix or exogenous growth factors might enhance donor cell engraftment after epicenter transplantation (Lu et al., 2014), although few studies have directly evaluated this issue, and the effect of trophic factors axon extension appears to be greater than that on overall neural progenitor engraftment (Bonner et al., 2011). In contrast, there was a significant inverse correlation between donor cell proliferation/expansion and transplantation dose. A similar inverse dose effect on donor cell proliferation using Ki67 antibody was reported by Ostenfeld et al. for PD at 2 WPT, but not by Darsalia et al. for stroke. In the immunodeficient SCI niche, donor cell expansion ranged from 16.3 fold (low dose) to 9.6 fold (very high dose) when normalized relative to the number of surviving cells at 2 WPT. Importantly, while these data represent significant cell

expansion, we calculate that as few as four divisions of each surviving human cell at 2 WPT would be sufficient to result in the numbers detected at 16 WPT (see Fig. 4B). Regardless of transplant dose, however, only 1–3% of the hCNS-SCns remained mitotic (that is, in M phase as detected by pH3) at 16 WPT, which is consistent with previous observations from our laboratory (Salazar et al., 2010) and others (Ostenfeld et al., 2000; Darsalia et al., 2011). Nonetheless, a critical remaining question is whether donor cell expansion dynamics involve a high degree of proliferation by a small number of human cells, or a fixed number of divisions by each engrafted donor cell. Understanding this dynamic relationship may reveal additional insight into the intrinsic and extrinsic factors defining donor cell proliferation and engraftment, and could inform strategies to improve the safety of cell therapeutics.

In accordance with our previous observations (Salazar et al., 2010), hCSN-SCns transplanted at the early-chronic stage of SCI exhibited migration away from the injury epicenter, as well as a preferential rostral localization in migration and proliferation. These data may suggest that extrinsic factors in the microenvironment influence the spatiotemporal dynamics of donor cell engraftment. Cell death induced neuroinflammation causes local upregulation of cytokines and chemokines, such as IL-8, SDF-1a, TNF-a as well as extracellular matrix proteins such as chondroitin sulfate proteoglygans (CSPGs) and integrins, which are crucial for guiding precursor migration and repair process (Leone et al., 2005; Connor et al., 2011; Brizzi et al., 2012; Dyck and Karimi-Abdolrezaee, 2015; Fawcett, 2015; North et al., 2015). In parallel, SCI results in a time-dependent regulation of the expression of trophic and regulatory factors such as ciliary neurotrophic factor (CNTF), FGF2, and glial growth factor 2 (GGF2), which can stimulate proliferation of endogenous precursor cells (Zai et al., 2005; Kumamaru et al., 2013). Interestingly, the highest FGF2 and GGF2 levels, and greatest chronic cell death, after SCI have been reported rostral to the epicenter (Shuman et al., 1997; Warden et al., 2001; Zai et al., 2005), perhaps suggesting that other ongoing injury dynamics could derive selective donor cell recruitment in a spatially dependent manner. Interestingly, increasing transplantation dose increased the number of donor cells localized in the caudal niche at 16 WPT, perhaps suggesting that donor cell density may in turn modulate SCI microenvironment by producing factors that stimulate migration of their sister cells, resulting in an increase in the distribution of donor cells throughout the tissue. Alternatively, as perhaps suggested by the plateau observed in hCNS-SCns engraftment, the number of integration sites adjacent to the injury and transplantation locus could have a limit, resulting in increased migration to distal regions once these closer sites are filled.

5. Conclusions

All together, these data suggest that the SCI niche may have a limited capacity to provide integration sites/growth signals for donor cells that can be detected as a change in dynamics of donor cell engraftment, expansion and migration. Critically, donor cell expansion was inversely regulated by target niche parameters and/or the initial donor cell density, highlighting that the response of transplanted cells to the host microenvironment should be a key variable in defining target dosing in pre-clinical models of CNS disease and injury.

Supplementary data to this article can be found online at http://dx.doi.org/10.1016/j.scr.2015.07.001.

Acknowledgments

We want to thank technical staff at Christopher and Dana Reeve Foundation Core (CDRF core), especially Rebecca Nishi, M.S., Hongli-Liu, M.D., Chelsea Pagan, B.S, Christina de Armond, B.S, and Elizabeth Hoffman, B.S, for their help with animal surgeries. We also thank Colleen Worne, B.S., and Eileen Do, B.S., for technical assistance. This study was supported in part by the National Institutes of Health (Grant U01NS079420) to A.J.A. and B.J.C.; the Christopher Reeve Foundation (AAC-2005) to A.J.A.; and by the CIRM Postdoctoral Training Grant (TG2-01152) to K.M.P.

References

Aguado, B., Mulyasasmita, W., Su, J., Lampe, K., Heilshorn, S., 2012. Improving viability of stem cells during syringe needle flow through the design of hydrogel cell carriers. Tissue Eng. A 18, 806–815.

Anderson, A., Haus, D., Hooshmand, M., Perez, H., Sontag, C., Cummings, B., 2011. Achieving stable human stem cell engraftment and survival in the CNS: is the future of regenerative medicine immunodeficient? Regen. Med. 6, 367–773.

Bakshi, A., Keck, C., Koshkin, V., LeBold, D., Siman, R., Snyder, E., McIntosh, T., 2005. Caspase-mediated cell death predominates following engraftment of neural progenitor cells into traumatically injured rat brain. Brain Res. 1065, 8–19.

Bonner, J.F., Connors, T.M., Silverman, W.F., Kowalski, D.P., Lemay, M.A., Fischer, I., 2011. Grafted neural progenitors integrate and restore synaptic connectivity across the injured spinal cord. J. Neurosci. 31, 4675–4686.

Brizzi, M.F., Tarone, G., Defilippi, P., 2012. Extracellular matrix, integrins, and growth factors as tailors of the stem cell niche. Curr. Opin. Cell Biol. 24.

Chen, B., Cui, X., Sempowski, G., Domen, J., Chao, N., 2004. Hematopoietic stem cell dose correlates with the speed of immune reconstitution after stem cell transplantation. Blood 103, 4344–4352.

Connor, B., Gordon, R.J., Jones, K.S., Maucksch, C., 2011. Deviating from the well travelled path: precursor cell migration in the pathological adult mammalian brain. J. Cell. Biochem. 112, 1467–1474.

Cummings, B., Uchida, N., Tamaki, S., Salazar, D., e., Hooshmand, M., Summers, R., Gage, F. and Anderson, A., 2005. Human neural stem cells differentiate and promote locomotor recovery in spinal cord-injured mice. Proc. Natl. Acad. Sci. U. S. A. 102, 14069–14143.

Cummings, B.J., Hooshmand, M.J., Salazar, D.L., Anderson, A.J., 2009. Human neural stem cell mediated repair of the contused spinal cord: timing the microenvironment. In: C. A. d. l. H., Ribak, Charles E., Jones, Edward G., Larriva Sahd, Jorge A., Swanson, Larry W. (Eds.), From Development to Degeneration and Regeneration of the Nervous System. Oxford University Press.

Darsalia, V., Allison, S., Cusulin, C., Monni, E., Kuzdas, D., Kallur, T.S., Lindvall, O., Kokaia, Z., 2011. Cell number and timing of transplantation determine survival of human neural stem cell grafts in stroke-damaged rat brain. J. Cereb. Blood Flow Metab. 31, 235–242.

Discher, D., Mooney, D., Zandstra, P., 2009. Growth factors, matrices, and forces combine and control stem cells. Science (New York, N.Y.) 324, 1673–1677.

Dyck, S.M., Karimi-Abdolrezaee, S., 2015. Chondroitin sulfate proteoglycans: key modulators in the developing and pathologic central nervous system. Exp. Neurol. 269, 169187.

Faigle, R., Song, H., 2013. Signaling mechanisms regulating adult neural stem cells and neurogenesis. Biochim. Biophys. Acta 1830, 2435–2448.

Fawcett, J.W., 2015. The extracellular matrix in plasticity and regeneration after CNS injury and neurodegenerative disease. Prog. Brain Res. 218, 213–226.

Gomer, R.H., Jang, W., Brazill, D., 2011. Cell density sensing and size determination. Develop. Growth Differ. 53, 482–494.

Gurley, L., D'Anna, J., Barham, S., Deaven, L., Tobey, R., 1978. Histone phosphorylation and chromatin structure during mitosis in Chinese hamster cells. Eur. J. Biochem./FEBS 84, 1–15.

Hatten, M., 1999. Central nervous system neuronal migration. Annu. Rev. Neurosci. 22, 511–550.

Hendzel, M., Wei, Y., Mancini, M., Van Hooser, A., Ranalli, T., Brinkley, B., Bazett-Jones, D., Allis, C., 1997. Mitosis-specific phosphorylation of histone H3 initiates primarily within pericentromeric heterochromatin during G2 and spreads in an ordered fashion coincident with mitotic chromosome condensation. Chromosoma 106, 348–360.

Hooshmand, M.J., Sontag, C.J., Uchida, N., Tamaki, S., Anderson, A.J., Cummings, B.J., 2009. Analysis of host-mediated repair mechanisms after human CNS-stem cell transplantation for spinal cord injury: correlation of engraftment with recovery. PLoS One 4, e5871.

Johnston, L., 2009. Competitive interactions between cells: death, growth, and geography. Science (New York, N.Y.) 324, 1679–1682.

Jones, D., Wagers, A., 2008. No place like home: anatomy and function of the stem cell niche. Nat. Rev. Mol. Cell Biol. 9, 11–21.

Keirstead, H.S., Nistor, G., Bernal, G., Totoiu, M., Cloutier, F., Sharp, K., Steward, O., 2005. Human embryonic stem cell-derived oligodendrocyte progenitor cell transplants remyelinate and restore locomotion after spinal cord injury. J. Neurosci. 25, 4694–4705.

Kill, I., 1996. Localisation of the Ki-67 antigen within the nucleolus. Evidence for a fibrillarin-deficient region of the dense fibrillar component. J. Cell Sci. 109 (Pt 6), 1253–1263.

Kumamaru, H., Saiwai, H., Kubota, K., Kobayakawa, K., Yokota, K., Ohkawa, Y., Shiba, K., Iwamoto, Y., Okada, S., 2013. Therapeutic activities of engrafted neural stem/precursor cells are not dormant in the chronically injured spinal cord. Stem Cells 31 (8), 1535–1547.

Leone, D.P., Relvas, J.B., Campos, L.S., Hemmi, S., Brakebusch, C., Fässler, R., Ffrench-Constant, C., Suter, U., 2005. Regulation of neural progenitor proliferation and survival by β1 integrins. J. Cell Sci. 118, 2589–2599.

Liu, C., Chen, B., Deoliveira, D., Sempowski, G., Chao, N., Storms, R., 2010. Progenitor cell dose determines the pace and completeness of engraftment in a xenograft model for cord blood transplantation. Blood 116, 5518–5527.

Lu, P., Woodruff, G., Wang, Y., Graham, L., Hunt, M., Wu, D., Boehle, E., Ahmad, R., Poplawski, G., Brock, J., Goldstein, L.S., Tuszynski, M.H., 2014. Long-distance axonal growth from human induced pluripotent stem cells after spinal cord injury. Neuron 83 (4), 789–796.

Lui, J.H., Hansen, D.V., Kriegstein, A.R., 2011. Development and evolution of the human neocortex. Cell 146 (1), 18–36.

McTigue, D., Wei, P., Stokes, B., 2001. Proliferation of NG2-positive cells and altered oligodendrocyte numbers in the contused rat spinal cord. J. Neurosci. Off. J. Soc. Neurosci. 21, 3392–3400.

North, H.A., Pan, L., McGuire, T.L., Brooker, S., Kessler, J.A., 2015. 1-Integrin alters ependymal stem cell bmp receptor localization and attenuates astrogliosis after spinal cord injury. J. Neurosci. 35, 37253733.

Ostenfeld, T., Caldwell, M., Prowse, K., Linskens, M., Jauniaux, E., Svendsen, C., 2000. Human neural precursor cells express low levels of telomerase in vitro and show diminishing cell proliferation with extensive axonal outgrowth following transplantation. Exp. Neurol. 164, 215–226.

Piltti, K., Salazar, D., Uchida, N., Cummings, B., Anderson, A., 2013a. Safety of epicenter versus intact parenchyma as a transplantation site for human neural stem cells for spinal cord injury therapy. Stem Cells Transl. Med. 2, 204–216.

Piltti, K., Salazar, D., Uchida, N., Cummings, B., Anderson, A., 2013b. Safety of human neural stem cell transplantation in chronic spinal cord injury. Stem Cells Transl. Med. 2, 961–974.

Piltti, K.M., Funes, G.M., Avakian, S.A., A, S. A., K, H., Uchida, N., Cummings, B.J., Anderson, A.J., 2015. Increasing Human Neural Stem Cell Transplantation Dose Alters Oligodendroglial and Neuronal Differentiation After Spinal Cord Injury (submitted for publication).

Prochazka, M., Gaskins, H., Shultz, L., Leiter, E., 1992. The nonobese diabetic scid mouse: model for spontaneous thymomagenesis associated with immunodeficiency. Proc. Natl. Acad. Sci. U. S. A. 89, 3290–3294.

Rossi, S., Nistor, G., Wyatt, T., Yin, H., Poole, A., Weiss, J., Gardener, M., Dijkstra, S., Fischer, D., Keirstead, H., 2010. Histological and functional benefit following transplantation of motor neuron progenitors to the injured rat spinal cord. PLoS One 5.

Salazar, D., Uchida, N., Hamers, F., Cummings, B., Anderson, A., 2010. Human neural stem cells differentiate and promote locomotor recovery in an early chronic spinal cord injury NOD-scid mouse model. PLoS One 5.

Shibata, K., Ajiro, K., 1993. Cell cycle-dependent suppressive effect of histone H1 on mitosis-specific H3 phosphorylation. J. Biol. Chem. 268, 18431–18434.

Shuman, S., Bresnahan, L., J., C. and Beattie, M., S., 1997. Apoptosis of microglia and oligodendrocytes after spinal cord contusion in rats. J. Neurosci. Res. 50.

Sontag, C., Nguyen, H., Kamei, N., Uchida, N., Anderson, A., Cummings, B., 2013. Immunosuppressants affect human neural stem cells in vitro but not in an in vivo model of spinal cord injury. Stem Cells Transl. Med. 2, 731–744.

Sontag, C., Uchida, N., Cummings, B., Anderson, A., 2014. Injury to the spinal cord niche alters the engraftment dynamics of human neural stem cells. Stem Cell Rep. 2, 620–632.

Tanaka, R., Tainaka, M., Ota, T., Mizuguchi, N., Kato, H., Urabe, S., Chen, Y., Fustin, J.-M., Yamaguchi, Y., Doi, M., Hamada, S., Okamura, H., 2011. Accurate determination of S-phase fraction in proliferative cells by dual fluorescence and peroxidase immunohistochemistry with 5-bromo-2′-deoxyuridine (BrdU) and Ki67 antibodies. J. Histochem. Cytochem. Off. J. Histochem. Soc. 59, 791–798.

Uchida, N., Buck, D.W., He, D., Reitsma, M.J., Masek, M., Phan, T.V., Tsukamoto, A.S., Gage, F.H., Weissman, I.L., 2000. Direct isolation of human central nervous system stem cells. Proc. Natl. Acad. Sci. U. S. A. 97, 14720–14725.

Voog, J., Jones, D., 2010. Stem cells and the niche: a dynamic duo. Cell Stem Cell 6, 103–115.

Wagers, A., 2012. The stem cell niche in regenerative medicine. Cell Stem Cell 10, 362–369.

Warden, P., Bamber, N., Li, H., Esposito, A., Ahmad, K., Hsu, C., Xu, X., 2001. Delayed glial cell death following Wallerian degeneration in white matter tracts after spinal cord dorsal column cordotomy in adult rats. Exp. Neurol. 168, 213–224.

Watt, F., Hogan, B., 2000. Out of Eden: stem cells and their niches. Science (New York, N.Y.) 287, 1427–1430.

Wilcock, A., Swedlow, J., Storey, K., 2007. Mitotic spindle orientation distinguishes stem cell and terminal modes of neuron production in the early spinal cord. Development (Cambridge, England) 134, 1943–1997.

Zai, L., Yoo, S., Wrathall, J., 2005. Increased growth factor expression and cell proliferation after contusive spinal cord injury. Brain Res. 1052, 147–155.